Significant contribution of HONO to secondary pollutants during a severe winter pollution event in southern China

Xiao Fu [a], Tao Wang [a, *], Li Zhang [a, b], Qinyi Li [a, **], Zhe Wang [a], Men Xia [a], Hui Yun [a], Weihao Wang [a], Chuan Yu [a], Dingli Yue [c], Yan Zhou [c], Junyun Zheng [d], Rui Han [e]

[a] Department of Civil and Environmental Engineering, Hong Kong Polytechnic University, Hong Kong 99907, China

[b] Atmospheric and Oceanic Sciences, Princeton University, Princeton, New Jersey 08540, United States

[c] Guangdong Provincial Environmental Monitoring Center, Guangzhou, China

[d] Institute for Environmental and Climate Research, Jinan University, Guangzhou, China

[e] National Meteorological Information Center, China Meteorological Administration, Beijing 100081, China

* *Correspondence to:* Tao Wang (tao.wang@polyu.edu.hk)

** Now at: Department of Atmospheric Chemistry and Climate, Institute of Physical Chemistry Rocasolano, CSIC, Madrid 28006, Spain

Abstract

Nitrous acid (HONO) can strongly affect atmospheric photochemistry in polluted regions through the production of hydroxyl radical (OH). In January 2017, a severe pollution episode occurred in the Pearl River Delta (PRD) of China, with maximum hourly $PM_{2.5}$, ozone and HONO levels reaching 400 μg/m^3, 150 ppb, and 8 ppb, respectively, at a suburban site. The present study investigated the sources/processes generating such high HONO concentrations and the role of HONO chemistry in this severe winter episode. Four recently reported HONO sources were added to the Community Multi-scale Air Quality (CMAQ) model, including RH-dependent and light-enhancing effects on heterogeneous reactions, photolysis of particulate nitrate in the atmosphere, and photolysis of HNO_3 and nitrate on surfaces. The revised model reproduced the observed HONO and significantly improved its performance for O_3 and $PM_{2.5}$. The model simulations showed that the heterogeneous generation on surfaces (with RH and light effects) was the largest contributor (72%) to the predicted HONO concentrations, with the RH-enhancing effects more significant at nighttime and the light-enhancing effects more important in the daytime. The photolysis of total nitrate in the atmosphere and deposited on surfaces was the dominant HONO source during noon and afternoon, contributing above 50% of the simulated HONO. The HONO photolysis was the dominant contributor to HO_X production in this episode. With all HONO sources, the daytime average O_3 at Heshan site was increased by 24 ppb (or 70%), compared to the simulation results without any HONO sources. Moreover, the simulated mean concentrations of TNO_3 (HNO_3 + fine particle NO_3^-) at Heshan site, which was the key species for this haze formation, increased by about 17 μg/m^3 (67%) due to the HONO chemistry, and the peak enhancement reached 55 μg/m^3. This study highlights the key role of HONO chemistry in the formation of winter haze in a subtropical environment.

1 Introduction

Nitrous acid (HONO) can significantly affect atmospheric photochemistry through its photolysis producing hydroxyl radical (OH) (R1) and subsequent reactions of OH with other gases (Alicke et al., 2003; Kleffmann et al., 2005). OH radical oxidizes volatile organic compounds (VOC) and converts nitric oxide (NO) into nitrogen dioxide (NO_2) without consuming ozone (O_3), leading to the generation of O_3 (R2 to R6). The oxidation of oxides of nitrogen (NO_X=NO+NO_2), sulfur dioxide (SO_2) and VOC by OH and O_3 also produce secondary aerosols, which are the key components of haze (e.g., Pathak et al., 2009; 2011; Cao et al., 2012).

$$HONO + h\nu \rightarrow NO + OH \quad (R1)$$

$$OH + VOC \rightarrow RO_2 + H_2O \quad (R2)$$

$$RO_2 + NO \rightarrow NO_2 + HO_2 + OVOC \quad (R3)$$

$$HO_2 + NO \rightarrow NO_2 + OH \quad (R4)$$

$$NO_2 + h\nu \rightarrow NO + O^3P \quad (R5)$$

$$O^3P + O_2 \rightarrow O_3 \quad (R6)$$

The impact of HONO on atmospheric photochemistry varies under different environmental conditions. In general, the effect of HONO is more significant in polluted conditions than clean conditions. For example, calculations constrained by field measurements of HONO have suggested that the contributions of HONO photolysis to the daytime HO_X (HO_X = OH + HO_2) production can reach 56% in an urban area (Ren et al., 2003) and 87% at a roadside (Yun et al., 2017), which are higher than the contributions in rural and forested areas (30% to 40%) (Acker et al., 2006; Kleffmann et al., 2005). Simulations by chemistry transport model which considered major sources of HONO showed that the maximum enhancements of O_3 concentrations due to HONO were mostly less than 10 ppb in the US and other western countries (Sarwar et al., 2008; Czader et al., 2012; Li et al., 2010; Goncalves et al., 2012), but more significant impacts have been reported in China due to more intense NO_X and VOC emissions. For example, the reported maximum hourly O_3 enhancement can be more than 30 ppb in Beijing (Li et al., 2011; Xu et al., 2006) and up to 25 ppb in Hong Kong (Zhang et al., 2016). The previous studies mostly focused on summertime.

Limited attention has been paid to the winter season when the observed HONO concentrations can also be high (Hou et al., 2016; Li et al., 2018a; Wang et al., 2016; Xu et al., 2015).

The source and formation mechanism of HONO are still not fully understood. Most previous studies suggest that heterogeneous reaction of NO_2 on surface is dominant, especially at night (Li et al., 2012; Wang et al., 2017a; Zhang et al., 2016). In the daytime, the long-known gas-phase reaction of NO and OH explains less than 10% of the daytime HONO production (Sarwar et al., 2008; Li et al., 2010; Zhang et al., 2016). Other daytime sources include direct traffic emissions (Kurtenbach et al., 2001; Liang et al., 2017), humidity and light-dependent heterogeneous generation (Finlayson-Pitts et al., 2003; Ndour et al., 2008; Monge et al., 2010), soil emissions (Oswald et al., 2013; Su et al., 2011; Meusel et al., 2018), photolysis of particle nitrate in the atmosphere (Ye et al., 2016b, 2017), and photolysis of deposited HNO_3 and nitrate on the ground (Ye et al., 2016a; Zhou et al., 2011), etc.

During 4-8 January 2017, a severe winter air pollution event occurred in the Pearl River Delta (PRD), a region long known to suffer from photochemical pollution due to its fast industrialization (Chan and Yao, 2008; Wang et al., 1998, 2003, 2017b; Xue et al., 2014; Zhang et al., 2008; Zheng et al., 2010). During this multi-day episode, an hourly peak value of ~150 ppb for O_3 and ~400 $\mu g/m^3$ for $PM_{2.5}$ were observed, and the HONO levels reached 8 ppb, with an average value of 2.9 ppb at night (18:00 to 6:00) and 2.4ppb in daytime (7:00 to 17:00). The HONO values were among the highest ever reported in China (Bernard et al., 2016; Huang et al., 2017; Li et al., 2012; Qin et al., 2009; Su et al., 2008; Wang et al., 2017a; Wang et al., 2013; Li et al., 2018a; Xu et., 2015). It is of great interest to find out how such a high level of HONO was produced and what impact it had on the radical levels and secondary pollutants during this severe winter pollution event.

The present study utilizes the CMAQ model with up-to-date HONO sources, including those in the original CMAQ model (gas-phase generation, heterogeneous reaction, and vehicle emissions) and four newly added sources (RH-enhancing effects on heterogeneous reactions, light-enhancing effects on heterogeneous reactions, photolysis of particulate nitrate in the atmosphere, and photolysis of HNO_3 and nitrate adsorbed on surfaces). The updated model was then used to analyze the contributions of different HONO sources, and also to

quantify the contributions of HONO to secondary pollutants during this severe winter pollution event. Our study reveals the very large impact of HONO on winter-time chemistry at this subtropical site.

2 Materials and Methods

2.1 Model description

2.1.1 CMAQ model configurations and inputs

CMAQ version 5.1 with the updated carbon bond 2005 e51 (CB05e51) gas mechanism and AERO6 aerosol mechanism (Appel et al., 2017) was used in this study. One-way triple nesting domains were used with their horizontal resolutions being 36, 12, and 4 km, respectively, and the innermost domain covers the PRD region (Fig. 1). These domains are based on a Lambert projection with two true latitudes of 25° N and 40° N. The objective simulation period was 4 to 8 January 2017, with six days before as a spin-up time.

The Weather Research & Forecasting Model (WRF) version 3.7 was applied to generate the meteorological fields for the CMAQ simulations. The physical options used in the WRF model were the Lin microphysics scheme (Lin et al., 1983), Rapid Radiative Transfer Model for GCMs (RRTMG) shortwave and longwave radiation scheme (Mlawer and Clough, 1998; Mlawer et al., 1997), Noah land surface scheme (Chen and Dudhia, 2001), YSU PBL scheme (Hong et al., 2006), and Kain–Fritsch cumulus scheme (Kain., 2004). To improve the meteorological modeling performance, the nudging was performed using the NCEP Automated Data Processing (ADP) data (ds351.0 and ds461.0) and surface observation data from China Meteorological Administration (Zhang et al., 2016). Table S1 summarizes the statistical performance for the meteorological predictions.

The anthropogenic emission input was generated based on three emission inventories covering different regions. For the PRD region, a local emission inventory with high resolution for 2010 (Pan et al., 2014) was used. For other regions in China, the emission data for 2013 were from Ma et al. (2017). For other Asian countries, the INTEX-B dataset (Zhang

et al., 2009) was used. HONO emissions from transportation sources were calculated based on the HONO/NO_X ratios and NO_X emissions from the transportation sources in the anthropogenic emission inventory. The HONO/NO_X ratios were set as 0.8% and 2.3% for gasoline and diesel engines, respectively (Kurtenbach et al., 2001; Gutzwiller et al., 2002). Natural biogenic emissions were estimated by the Model of Emissions of Gases and Aerosols from Nature (MEGAN) (Guenther et al., 2006).

2.1.2 Parameterization of HONO Sources

In addition to the direct anthropogenic emissions, the default CMAQ model has two HONO more sources, including the gas-phase homogeneous reaction of NO and OH (R7) and the heterogeneous reactions of NO_2 on surfaces (R8) (Sarwar et al., 2008). The heterogeneous formation of HONO on the surfaces of particle, urban and leaves was estimated with a reaction rate $k = 5 \times 10^{-5} \times (S/V)$ as measured by Kurtenbach et al. (2001) under dark conditions with a relative humidity (RH) of 50%.

$$NO + OH \rightarrow HONO \qquad \text{(R7)}$$

$$2NO_2 + H_2O \xrightarrow{surface} HONO + HNO_3 \qquad \text{(R8)}$$

In the present study, we incorporated four additional HONO sources, as described below.

(1) RH-enhancing effects on heterogeneous reaction of NO_2 on surfaces

The default heterogeneous reaction rate was based on measurements at a relative humidity of 50%. However, previous field and lab studies found that surface adsorbed water played a key role in the heterogeneous conversion and the reaction rate was highly dependent on the RH level (Finlayson-Pitts et al., 2003; Stutz et al., 2004; Qin et al., 2009). The laboratory measurements over an RH range of 0% to 80% conducted by Finlayson-Pitts et al. (2003) showed that the heterogeneous conversion rate increased much faster when RH≥50% than that when RH<50%. Based on this result, the RH dependence of the heterogeneous reaction was considered through scaling the default reaction rate by a factor of f_{RH} in this study, as shown in the following equation:

$$k_{het} = 5 \times 10^{-5} \times f_{RH} \times (S/V) \qquad \text{(E1)}$$

156 $$f_{RH}=\begin{cases} RH/50 & (RH<50) \\ RH/10-4 & (50\le RH<80) \\ 4 & (RH\ge 80) \end{cases}$$

157 **(2) Light-enhancing effects on heterogeneous reaction of NO_2 on surfaces**

158 The default reaction rate coefficient for the heterogeneous reaction was based on
159 measurements under dark conditions. However, it has been reported that sunlight significantly
160 boosts the heterogeneous generation of HONO (Ndour et al., 2008; Monge et al., 2010;
161 Stemmler et al., 2007). To consider the photo-enhancing effect, we applied a higher reaction
162 rate at daytime (Li et al., 2010; Czader et al., 2012), as shown in the following equation:

163 $$k_{het}=1\times10^{-3}\times\frac{light\ intensity}{400}\times(S/V) \qquad \text{(E2)}$$

164 where light intensity means the total downward irradiance at the surface, measured in watts per
165 meter squared (W/m^2).

166 **(3) Photolysis of particulate nitrate in the atmosphere**

167 Evidence from recent aircraft observations and laboratory measurements suggested that
168 particulate nitrate in the atmosphere can undergo photolysis to produce HONO and NO_2 (R9)
169 (Ye et al., 2016b, 2017).

170 $$pNO_3 \rightarrow 0.67\,HONO + 0.33\,NO_2 \qquad \text{(R9)}$$

171 Ye et al. (2017) reported the photolysis rates ranging from 6.2×10^{-6} s^{-1} to 5.0×10^{-4} s^{-1},
172 with a median of 8.3×10^{-5} s^{-1}, at noontime tropical conditions. The reported value was much
173 higher than the photolysis rate of gaseous HNO_3 ($\sim 7\times10^{-7}$ s^{-1}) under the typical tropical
174 noontime conditions (Finlayson-Pitts and Pitts., 2000; Ye et al., 2017). Similar to the
175 methodology of Sarwar et al. (2008), the photolysis rate of particulate nitrate was estimated as
176 the following equation:

177 $$J_{PNO3}=\frac{8.3\times10^{-5}}{7\times10^{-7}}\times J_{HNO3\text{-}CMAQ} \qquad \text{(E3)}$$

178 where $J_{HNO3\text{-}CMAQ}$ is the photolysis rate of gaseous HNO_3 calculated online in CMAQ.

179 **(4) Photolysis of HNO_3/nitrate deposited on surfaces**

180 Field observations and lab studies also indicated that the photolysis of HNO_3/nitrate
181 deposited on the surface could be an important daytime HONO source (R10) (Zhou et al.,
182 2003, 2011; Baergen et al., 2013). Ye et al. (2016a) tested the photolysis of HNO_3/nitrate

deposited on various natural and artificial surfaces in the laboratory, and reported the photolysis rates ranging from 6×10^{-6} s^{-1} to 3.7×10^{-4} s^{-1}, with a median of 3.4×10^{-5} s^{-1}.

$$deposited\ \_HNO_3 / nitrate \rightarrow 0.67\,HONO + 0.33\,NO_2 \quad \text{(R10)}$$

This reaction was incorporated into the CMAQ model by assuming deposited HNO_3/nitrate on surfaces to equal the accumulation of dry deposition since the last precipitation event, referring to the method of Sarwar et al. (2008). The photolysis rate of deposited HNO_3/nitrate was estimated as the following equation:

$$J_{DNO3} = \frac{3.4\times10^{-5}}{7\times10^{-7}} \times J_{HNO3\text{-}CMAQ} \quad \text{(E4)}$$

2.1.3 Simulation cases

Eight simulations were conducted considering different HONO sources, including:

NO_HONO: without any HONO sources

G: gas-phase homogeneous reaction (G)

GE: G + vehicle emissions (E)

GEH (CMAQ-default): GE + heterogeneous reactions under dark conditions with a RH of 50% (H)

GEHR: GEH + RH-enhancing effects on heterogeneous reactions (R)

GEHRL: GEHR + light-enhancing effects on heterogeneous reactions (L)

GEHRLP: GEHRL + photolysis of particulate nitrate in the atmosphere (P)

GEHRLPD (CMAQ-revised): GEHRLP + photolysis of HNO_3/nitrate deposited on the surface (D)

2.2 Observation data

Field observations of HONO and other major air pollutants were conducted at Heshan site (112°55′17″E, 22°42′50″N) in the PRD region (Fig. 1). Hourly HONO concentration was measured using a Long Path Absorption Photometer (LOPAP) (QUMA, Model LOPAP-03) (Heland et al., 2001). The same instrument was employed by our group in several previous field campaigns (Zha et al., 2014; Xu et al., 2015; Liang et al., 2017; Yun et al., 2018). The reader to

refered to these sources (e.g., Yun et al., 2018) for description of measurement principle. Following our previous practice, the instrument background was determined with synthetic air 4 times a day, and calibrations with a nitrite soluation standard were conducted every 3 days. The time resolution of this instrument was 10 min. The detection limit was 7 ppt with an accuracy of ±20%. The sample inlets were placed at the roof of a 4-floor building, at a height of about 15 m above the ground.

Other instruments whose data are used in the present paper have been summarized in Yun et al. (2018) with references provided for each instrument. Briefly, $PM_{2.5}$ concentrations were determined by a Multi Angle Absorption Photometer (Thermo Scientific, Model 5012). Sulfate, nitrate and ammonium in $PM_{2.5}$ were measured by a gas and aerosol collector coupled with an ion chromatography (GAC-IC) system. Gas HNO_3 concentrations were also measured by this GAC-IC system. O_3 concentrations were measured by a UV photometric analyzer (Thermo Scientific, Model 49i). NO_2 concentrations were measured using a chemiluminescence instrument (Thermo Scientific, Model 42i) coupled with a photolytic converter (Droplet Measurement Technologies, model BLC). The sample inlets for these instruments were placed at the same height as LOPAP.

Additionally, hourly $PM_{2.5}$, O_3 and NO_2 observation data at 56 official monitoring sites (Fig.1) in the PRD region were obtained from the Ministry of Environmental Protection (MEP). It should be noted that NO_2 concentrations in the national network were measured using the catalytic conversion method, which overestimates NO_2, especially during the period with active photochemistry and at the location away from the primary emission sources (Xu et al., 2013). The NO_2 observation data were adjusted based on the method of Zhang et al. (2017) (also see footnote of Table 1).

3 Results and Discussion

3.1 Observed pollution in this winter episode

During 4-8 January 2017, a severe pollution episode was observed in the PRD region. As shown in Fig. S1, the episode average $PM_{2.5}$ concentrations observed at the Heshan site

reached 142 μg/m^3, which is nearly twice the respective standard of China (75 μg/m^3 for daily average $PM_{2.5}$ concentration). The hourly $PM_{2.5}$ concentration peaked at 382 μg/m^3, which was among the highest $PM_{2.5}$ concentrations reported so far in the PRD region (Tan et al., 2009; Wang et al., 2012; Yue et al., 2015). O_3 levels were also high, with a peak of ~150ppb. Fig. S2 presented the spatial distribution of observed $PM_{2.5}$ and O_3 on the two heaviest polluted days (5 and 6 January) based on the interpolation of the observation data at the 56 official monitoring sites. It can be seen that the whole western PRD region suffered from severe pollution. On 5 January, the highest $PM_{2.5}$ pollution occurred in Foshan city and its surrounding area, with a peak of 448 μg/m^3. On 6 January, the pollution expanded to wider areas.

3.2 Evaluation of model performance

Figure 2 compared the simulated HONO mixing ratios by the default CMAQ model (GEH) and the revised CMAQ model (GEHRLPD) with the observations at Heshan site for 4-8 January. For the HONO simulation, the default CMAQ significantly underestimated the levels, with a normalized mean bias (NMB) of -71.6%. The maximum underestimation was 6ppb in the early morning of 5 January. The simulated HONO levels in the afternoon were lower than 0.1 ppb in the default CMAQ model. By considering the four additional HONO sources, the model performance was improved considerably, with an NMB of -22.5%. The simulated average daytime HONO mixing ratios increased from 0.37 to 1.44 ppb, and the simulated nighttime HONO values increased from 1.10 to 2.63 ppb. The revised model reproduced the HONO diurnal variation. Underestimation was found on the morning of 5-6 and 8 January. One possible reason was that some HONO sources were not considered in this study. For example, previous studies have proposed that deposited HONO can be reserved in dew water on the ground or vegetation during the nighttime and re-released when the dew water evaporate in the morning (He et al., 2006). Here we have simply estimated HONO released from dew in the morning on 5 January when dew existed during 0:00-8:00 using the method described in He et al, (2006). The total HONO dry deposition was 1.28×10^{-6} moles/m^2. At 9:00, if 80% of accumulated HONO was emitted to the surface model layer (about 0-30m),

the total released HONO amount would be 0.76 ppb. This suggests that dew evaporation may be a considerable source, but other sources may also exist. Overestimation was seen at the nighttime of 4 and 7 January, which was possibly related to some missing HONO sinks, e.g. the uptake of HONO on the ground surface (VandenBoer et al., 2014). Additionally, the overestimation of NO_2 could also explain partially the overestimation of HONO at the nighttime of 7 January.

The inclusion of the four additional HONO sources also changed the model performance for other air pollutants. As shown in Fig. S1, the O_3 prediction by the default CMAQ model was not satisfactory, especially for the peak value. For example, on 6 January, the observed maximum 1-h and 8-h O_3 mixing ratios at Heshan site reached 147 ppb and 125 ppb, respectively, exceeding the respective standard of China (~93 ppb and 75 ppb for maximum 1-h and 8-h O_3 concentrations, respectively). The simulated levels by the default CMAQ model were just 64ppb and 52ppb, respectively, which failed to predict the non-compliance of O_3 for this episode. In contrast, the revised model was better to reproduce the magnitude. For the episode average, the NMB values decreased from -32.9% to 5.5% for the maximum 8-h O_3. Therefore, it is crucial to include these additional HONO sources into air quality models. For NO_2, the revised model could reproduce its temporal variation in general, although underestimation was seen for some peak NO_2 values. This under-prediction could also explain partially the underestimation of HONO peak values. For $PM_{2.5}$, improvements also can be seen, especially for the peak values. For the sulfate, nitrate and ammonium components in $PM_{2.5}$, as shown in Fig.S3, the revised model performed well in reproducing their temporal variations, with correlation coefficients (R value) of 0.5, 0.7 and 0.7, respectively. Compared to the default CMAQ model, the NMB values decreased from -29.8% to -10%, -53.8% to -41.2%, and -32.9% to -14.1% for fine particle sulfate, nitrate and ammonium, respectively. Underestimation could be seen for particle nitrate, especially on 5 January. The possible reason was underestimation of the emissions of NH_3 or other alkaline species (e.g. Ca, K, Na), which led to gas HNO_3 not being converted to particle nitrate sufficiently. The model performance for total nitrate (TNO_3 = gaseous HNO_3 + fine particle nitrate) was satisfactory, with an NMB of -3.2% and R of 0.8.

Regionally, as shown in Table 1, the simulation results of the revised CMAQ model

were in better agreement with the observations, with the NMBs decreasing from -33.3% to 0.7%, -8.1% to 4.7%, and 20.6% to 9.4% for 8-hour maximum O_3, hourly average $PM_{2.5}$ and hourly average NO_2 values, respectively.

We have conducted a sensitivity test to compare the simulations with those considering more recent emission by linearly adjusting the emissions based on the ratio of 2017 emission to 2010 emission for China reported in a very recent paper (Zheng et al., 2018), but no improvements were indicated for HONO, O_3, and $PM_{2.5}$ at the Heshan site (Fig. S4). Despite the uncertainty, we think that the current emission setting is acceptable for simulations of the present case.

The above results indicated the satisfactory performance of the revised CMAQ model to simulate HONO and other major pollutants. It could be used to analyze the formation and impact of HONO in this episode.

3.3 Contributions of different sources to HONO concentrations

Figure 3 presents the contributions of different HONO sources to the HONO mixing ratios at Heshan site. Heterogeneous generation on surfaces (including RH and light effects, H+R+L) was the largest contributor, representing 72% of the average predicted HONO for the whole day. It contributed up to 81% of the average predicted HONO values during the nighttime (18:00 to 6:00) and ~52% during the daytime (7:00 to 17:00). These findings on the dominant contribution from heterogeneous generation were similar to those in the previous modeling studies (Sarwar et al., 2008; Zhang et al., 2016) and field measurements (Li et al., 2012; Wang et al., 2017a). High relative humidity and solar radiation were two important driving factors for the formation of the high HONO concentrations in this pollution episode. During the nighttime and early morning (18:00 to 8:00), RH-enhancing effects on the heterogeneous generation were significant, due to high relative humidity (70% to 90%) (Fig. S5). The heterogeneous generation of HONO had a ~2-fold increase by considering RH-enhancing effects, compared to that under the uniform relative humidity of 50%. From 9:00 to the afternoon, light-enhancing effects became important, contributing approximately 25% to HONO levels, due to strong radiation with a maximum of ~450 W/m^2 (Fig. S5). In

addition to enhancing the heterogeneous generation, the existence of light also increased HONO values through the photolysis of particle nitrate in the atmosphere and total nitrate deposited on the surface. Due to the high total nitrate concentrations in this pollution episode, these two photolysis sources were dominant during noon and afternoon (11:00 to 17:00), contributing 31% and 36% to the HONO levels, respectively. Vehicle emissions contributed approximately 8% of the daily average HONO values. The gas-phase homogeneous reaction was the smallest source, contributing approximately 3% and 7% of the daily and daytime average HONO values, respectively. Our model simulations suggest that the three additional light-dependent sources (L+P+D) could be an important part of missing daytime sources for the present case.

3.4 Impacts of HONO chemistry on HO_X and O_3

The HO_X ($OH+HO_2$) radical plays a key role in the atmospheric photochemical process. The photolysis of HONO can produce OH radical, and fast conversion exists between OH and HO_2 radical. Therefore, the photolysis of HONO can affect the abundance of HO_X radical. Figure 4 presents the average diurnal OH and HO_2 variations based on the simulations with and without the HONO sources (NO_HONO vs. GEHRLPD). The diurnal pattern and magnitude of the simulated OH and HO_2 mixing ratios in the GEHRLPD case were comparable to the previous observations in the PRD region and other areas (Lu et al., 2012; Mao et al., 2010). Compared to the results of the NO_HONO simulation, the daytime average OH and HO_2 values were increased by 175% and 336%, respectively. The integrated reaction rate (IRR) analysis tool available in CMAQ was utilized to explore the contribution of HONO photolysis to HO_X radical production relative to other HO_X radical sources in the surface layer (~0 to 30 m), including the reaction of H_2O with O (1D) which comes from the photolysis of O_3, HCHO photolysis, H_2O_2 photolysis, and the reaction of O_3 with alkenes and biogenic VOCs. As shown in Fig. 5, HONO photolysis was the dominant HO_X source during the daytime at Heshan site. The daytime average contribution of HONO photolysis to HO_X production was approximately 74%, and the contribution during the morning could be above 90%. With the increasing of O_3 concentrations from sunrise to afternoon, the contribution of

the O_3 photolysis began to increase and reached a peak of 33.4% at 14:00. Compared to the reported results for summer in the previous studies (Czader et al., 2012; Mao et al., 2010; Tham et al., 2016; Xue et al., 2016; Li et al., 2018c), the contribution of HONO photolysis to HO_X was much larger in the present study, mainly due to the high HONO concentrations in this winter episode. For example, Xue et al. (2016) and Li et al. (2018c) reported daytime average contributions of less than 30% from HONO photolysis at two sites in Hong Kong. Tham et al. (2016) showed a contribution of less than 50% in the morning at a site in the North China Plain. In these cases, the HONO levels were relatively low, with the peak HONO levels ranging among 1-3ppb. The high HONO concentrations at Heshan increased the contribution of HONO photolysis to the formation of HO_X in this winter pollution episode. The similar high contribution can be found in other winter studies with high HONO concentrations, e.g. Elshorbany et al. (2010).

The enhanced HO_X formation due to HONO chemistry could increase O_3 concentrations. As shown in Fig. 6, the simulated daytime average O_3 mixing ratio at Heshan site in the GEHRLPD case was approximately 24 ppb (70%) higher than that in the NO_HONO case, with a peak increase up to 60 ppb. The O_3 enhancement was much higher than the previous simulation results for the summer cases (Sarwar et al., 2008; Li et al., 2010; Zhang et al., 2016). In addition to higher HONO concentrations, another possible reason was that the VOC/NO_X ratio was lower in winter than that in summer, due to less biogenic VOC emissions and more NO_X emission from fuel combustion in winter. For example, Zou et al. (2015) reported VOC/NO_X values higher than 10:1 in summer and about 5:1 for winter based on 1-year observation in Guangzhou, which is about 60 km from the Heshan site. The lower VOC/NO_X ratio increased the sensitivity of O_3 concentrations to HO_X changes through reaction 2 to 4. Therefore, the enhancement of O_3 concentrations was more significant (Li et al., 2018b). Figure 7 presents the spatial distribution of simulated surface O_3 concentrations at 15:00 LTC in the NO_HONO and GEHRLPD cases. With HONO sources, the increase of regional average O_3 mixing ratio at 15:00 LTC was 34% (~17 ppb). The above results indicated the significant impacts of HONO chemistry on the atmospheric oxidation capacity and O_3 pollution in the PRD region during this heavy winter episode.

3.5 Impacts of HONO chemistry on secondary inorganic aerosol formation

Secondary inorganic aerosols, including nitrate, sulfate and ammonium, contributed approximately 50% to $PM_{2.5}$ concentrations during this episode (Fig. S6). Among them, nitrate was the dominant component, with peak concentrations reaching ~110 $\mu g/m^3$, which was much higher than the sulfate and ammonium concentrations. Particle nitrate can be generated through the partition of HNO_3 to particle phase. The major formation pathway of HNO_3 is the oxidation of NO_2 by OH during the daytime (R11). HNO_3 can also be produced via heterogeneous reactions of N_2O_5 on the particle surface at night (R12 to R14). Therefore HONO chemistry can accelerate the formation of nitrate through the enhancement of atmospheric oxidation capacity (HO_X and O_3).

$$OH + NO_2 \rightarrow HNO_3 \qquad (R11)$$

$$O_3 + NO_2 \rightarrow NO_3 \qquad (R12)$$

$$NO_3 + NO_2 \rightarrow N_2O_5 \qquad (R13)$$

$$N_2O_5 + H_2O \rightarrow 2HNO_3 \qquad (R14)$$

Considering the uncertainty of the partition of gaseous HNO_3 to particle nitrate (see section 3.2), we assessed the impact of HONO chemistry on the sum of HNO_3 and fine particle NO_3^- (TNO_3). As shown in Fig. 8, the average TNO_3 concentrations at Heshan site increased by about 17 $\mu g/m^3$ (67%), and the peak enhancement reached 55 $\mu g/m^3$ at 10 am on January 6, when the observed $PM_{2.5}$ and nitrate concentration was at its respective highest level. Figure 9 presents the distribution of simulated average surface TNO_3 concentrations in the NO_HONO and GEHRLPD case. With HONO sources, the regional average TNO_3 concentrations were increased by 8.4 $\mu g/m^3$ for the entire episode. The absolute enhancement was more significant in the areas with higher aerosol concentrations. The highest increase for TNO_3 was above 25 $\mu g/m^3$ for the episode average. Meanwhile, the HONO chemistry also accelerated the formation of other secondary inorganic aerosols. Particle sulfate can be generated through the partition of H_2SO_4 to the particle phase. The major formation pathways of H_2SO_4 include the gaseous oxidation of SO_2 by OH, and the aqueous oxidation of S(IV) by O_3, H_2O_2 and other oxidants. The partition of gaseous NH_3 to particle ammonium was based on the H_2SO_4-HNO_3-NH_3 thermodynamic equilibrium. The simulated enhancements of the

average sulfate and ammonium concentrations at Heshan site were 32% and 33%, respectively. The above results indicated that the HONO chemistry also aggravated the particulate pollution during this episode.

4 Conclusion

This study has identified the major contributors to the observed high HONO levels during a severe winter pollution episode and highlighted the importance of HONO chemistry in the combined photochemical and haze pollution in a subtropical region. Including up-to-date HONO sources in the widely used CMAQ model significantly improved its capability in simulating ambient concentrations of HONO and other major pollutants (e.g. O_3 and $PM_{2.5}$). The model simulations suggested a predominant contribution from NO_2 heterogeneous reactions enhanced by humidity and solar radiation. The high HONO concentration significantly increased the atmospheric oxidation capacity and the levels of ozone and secondary aerosols, especially total nitrate. This study highlights the key role of HONO chemistry in the formation of winter haze in a subtropical environment and indicates the critical need to include/update HONO sources in regional air quality models in order to predict ozone and other secondary pollutants during heavy pollution events in southern China and similar regions. Additional efforts are needed to improve current representaiton of HONO sources such as evapation of dew and more accurate simulation of deposited nitrate.

Data availability

Model codes and input data are available from Xiao Fu. The measurement data used in this study are available from Tao Wang (cetwang@polyu.edu.hk) and Dingli Yue (dingliyue@163.com).

Author contributions

TW and XF designed the research; XF performed model similations and analysis; LZ and QL assisted in model simulations; YZ, DY, ZW, HY, MX, CY and WW conducted measurements of trace gases and aerosol; JZ processed the PRD emission data; RH processed the weather data.

XF and TW wrote the manuscript. All authors contributed to discussion and commented on the paper.

***Acknowledgments*.** We thank Miss Naiwen Zhang for her help in HONO measurement and the Environmental Protection Department of Hong Kong for loaning the LOPAP instrument. This work was sponsored by the Hong Kong Research Grants Council (C5022-14G and A-PolyU502/16).

References

Acker, K., Moller, D., Wieprecht, W., Meixner, F. X., Bohn, B., Gilge, S., Plass-Dulmer, C., and Berresheim, H.: Strong daytime production of OH from HNO2 at a rural mountain site, Geophysical Research Letters, 33, 10.1029/2005gl024643, 2006.

Alicke, B., Geyer, A., Hofzumahaus, A., Holland, F., Konrad, S., Patz, H. W., Schafer, J., Stutz, J., Volz-Thomas, A., and Platt, U.: OH formation by HONO photolysis during the BERLIOZ experiment, Journal of Geophysical Research-Atmospheres, 108, 10.1029/2001jd000579, 2003.

Appel, K. W., Napelenok, S. L., Foley, K. M., Pye, H. O. T., Hogrefe, C., Luecken, D. J., Bash, J. O., Roselle, S. J., Pleim, J. E., Foroutan, H., Hutzell, W. T., Pouliot, G. A., Sarwar, G., Fahey, K. M., Gantt, B., Gilliam, R. C., Heath, N. K., Kang, D., Mathur, R., Schwede, D. B., Spero, T. L., Wong, D. C., and Young, J. O.: Description and evaluation of the Community Multiscale Air Quality (CMAQ) modeling system version 5.1, Geoscientific Model Development, 10, 1703-1732, 10.5194/gmd-10-1703-2017, 2017.

Baergen, A. M., and Donaldson, D. J.: Photochemical Renoxification of Nitric Acid on Real Urban Grime, Environmental Science & Technology, 47, 815-820, 10.1021/es3037862, 2013.

Bernard, F., Cazaunau, M., Grosselin, B., Zhou, B., Zheng, J., Liang, P., Zhang, Y. J., Ye, X. N., Daele, V., Mu, Y. J., Zhang, R. Y., Chen, J. M., and Mellouki, A.: Measurements of nitrous acid (HONO) in urban area of Shanghai, China, Environmental Science and Pollution Research, 23, 5818-5829, 10.1007/s11356-015-5797-4, 2016.

Cao, J.-J., Shen, Z.-X., Chow, J. C., Watson, J. G., Lee, S.-C., Tie, X.-X., Ho, K.-F., Wang, G.-H., and Han, Y.-M.: Winter and Summer PM2.5 Chemical Compositions in Fourteen Chinese Cities, J. Air Waste Manage. Assoc., 62, 1214-1226, 10.1080/10962247.2012.701193, 2012.

Chan, C. K., and Yao, X.: Air pollution in mega cities in China, Atmospheric Environment, 42, 1-42, 10.1016/j.atmosenv.2007.09.003, 2008.

Chen, F., and Dudhia, J.: Coupling an advanced land surface-hydrology model with the Penn State-NCAR MM5 modeling system. Part I: Model implementation and sensitivity, Monthly Weather Review, 129, 569-585, 10.1175/1520-0493(2001)129<0569:caalsh>2.0.co;2, 2001.

Czader, B. H., Rappengluck, B., Percell, P., Byun, D. W., Ngan, F., and Kim, S.: Modeling nitrous acid and its impact on ozone and hydroxyl radical during the Texas Air Quality Study 2006, Atmospheric Chemistry and Physics, 12, 6939-6951, 10.5194/acp-12-6939-2012, 2012.

Elshorbany, Y. F., Kleffmann, J., Kurtenbach, R., Lissi, E., Rubio, M., Villena, G., Gramsch, E., Rickard, A. R., Pilling, M. J., and Wiesen, P.: Seasonal dependence of the oxidation capacity of the city of Santiago de Chile, Atmospheric Environment, 44, 5383-5394, 10.1016/j.atmosenv.2009.08.036, 2010.

Finlayson-Pitts, B. J., and Pitts, J. N., Jr. : Chemistry of the Upper and Lower Atmosphere: Theory, Experiments, and Applications, Academic Press, San Diego, CA, 2000.

Finlayson-Pitts, B. J., Wingen, L. M., Sumner, A. L., Syomin, D., and Ramazan, K. A.: The

heterogeneous hydrolysis of NO2 in laboratory systems and in outdoor and indoor atmospheres: An integrated mechanism, Physical Chemistry Chemical Physics, 5, 223-242, 10.1039/b208564j, 2003.

Goncalves, M., Dabdub, D., Chang, W. L., Jorba, O., and Baldasano, J. M.: Impact of HONO sources on the performance of mesoscale air quality models, Atmospheric Environment, 54, 168-176, 10.1016/j.atmosenv.2012.02.079, 2012.

Guenther, A., Karl, T., Harley, P., Wiedinmyer, C., Palmer, P. I., and Geron, C.: Estimates of global terrestrial isoprene emissions using MEGAN (Model of Emissions of Gases and Aerosols from Nature), Atmospheric Chemistry and Physics, 6, 3181-3210, 10.5194/acp-6-3181-2006, 2006.

Gutzwiller, L., Arens, F., Baltensperger, U., Gaggeler, H. W., and Ammann, M.: Significance of semivolatile diesel exhaust organics for secondary HONO formation, Environmental Science & Technology, 36, 677-682, 10.1021/es015673b, 2002.

He, Y., Zhou, X. L., Hou, J., Gao, H. L., and Bertman, S. B.: Importance of dew in controlling the air-surface exchange of HONO in rural forested environments, Geophysical Research Letters, 33, 10.1029/2005gl024348, 2006.

Heland, J., Kleffmann, J., Kurtenbach, R., and Wiesen, P.: A new instrument to measure gaseous nitrous acid (HONO) in the atmosphere, Environmental Science & Technology, 35, 3207-3212, 10.1021/es000303t, 2001.

Hong, S. Y., Noh, Y., and Dudhia, J.: A new vertical diffusion package with an explicit treatment of entrainment processes, Monthly Weather Review, 134, 2318-2341, 10.1175/mwr3199.1, 2006.

Hou, S., Tong, S., Ge, M., and An, J.: Comparison of atmospheric nitrous acid during severe haze and clean periods in Beijing, China, Atmospheric Environment, 124, 199-206, 10.1016/j.atmosenv.2015.06.023, 2016.

Huang, R. J., Yang, L., Cao, J. J., Wang, Q. Y., Tie, X. X., Ho, K. F., Shen, Z. X., Zhang, R. J., Li, G. H., Zhu, C. S., Zhang, N. N., Dai, W. T., Zhou, J. M., Liu, S. X., Chen, Y., Chen, J., and O'Dowd, C. D.: Concentration and sources of atmospheric nitrous acid (HONO) at an urban site in Western China, Science of the Total Environment, 593, 165-172, 10.1016/j.scitotenv.2017.02.166, 2017.

Kain, J. S.: The Kain-Fritsch convective parameterization: An update, Journal of Applied Meteorology, 43, 170-181, 10.1175/1520-0450(2004)043<0170:tkcpau>2.0.co;2, 2004.

Kleffmann, J., Gavriloaiei, T., Hofzumahaus, A., Holland, F., Koppmann, R., Rupp, L., Schlosser, E., Siese, M., and Wahner, A.: Daytime formation of nitrous acid: A major source of OH radicals in a forest, Geophysical Research Letters, 32, 10.1029/2005gl022524, 2005.

Kurtenbach, R., Becker, K. H., Gomes, J. A. G., Kleffmann, J., Lorzer, J. C., Spittler, M., Wiesen, P., Ackermann, R., Geyer, A., and Platt, U.: Investigations of emissions and heterogeneous formation of HONO in a road traffic tunnel, Atmospheric Environment, 35, 3385-3394, 10.1016/s1352-2310(01)00138-8, 2001.

Li, D., Xue, L., Wen, L., Wang, X., Chen, T., Mellouki, A., Chen, J., and Wang, W.: Characteristics and sources of nitrous acid in an urban atmosphere of northern China: Results from 1-yr continuous observations, Atmospheric Environment, 182, 296-306, 10.1016/j.atmosenv.2018.03.033, 2018a.

Li, G., Lei, W., Zavala, M., Volkamer, R., Dusanter, S., Stevens, P., and Molina, L. T.: Impacts of HONO sources on the photochemistry in Mexico City during the MCMA-2006/MILAGO Campaign, Atmospheric Chemistry and Physics, 10, 6551-6567, 10.5194/acp-10-6551-2010, 2010.

Li, Q., Zhang, L., Wang, T., Wang, Z., Fu, X., and Zhang, Q.: "New" Reactive Nitrogen Chemistry Reshapes the Relationship of Ozone to Its Precursors, Environmental Science & Technology, 52, 2810-2818, 10.1021/acs.est.7b05771, 2018b.

Li, X., Brauers, T., Haseler, R., Bohn, B., Fuchs, H., Hofzumahaus, A., Holland, F., Lou, S., Lu, K. D., Rohrer, F., Hu, M., Zeng, L. M., Zhang, Y. H., Garland, R. M., Su, H., Nowak, A., Wiedensohler, A., Takegawa, N., Shao, M., and Wahner, A.: Exploring the atmospheric chemistry of nitrous acid (HONO) at a rural site in Southern China, Atmospheric Chemistry and Physics, 12, 1497-1513, 10.5194/acp-12-1497-2012, 2012.

Li, Y., An, J., Min, M., Zhang, W., Wang, F., and Xie, P.: Impacts of HONO sources on the air quality in Beijing, Tianjin and Hebei Province of China, Atmospheric Environment, 45, 4735-4744, 10.1016/j.atmosenv.2011.04.086, 2011.

Li, Z., Xue, L., Yang, X., Zha, Q., Tham, Y. J., Yan, C., Louie, P. K. K., Luk, C. W. Y., Wang, T., and Wang, W.: Oxidizing capacity of the rural atmosphere in Hong Kong, Southern China, Science of the Total Environment, 612, 1114-1122, 10.1016/j.scitotenv.2017.08.310, 2018c.

Liang, Y. T., Zha, Q. Z., Wang, W. H., Cui, L., Lui, K. H., Ho, K. F., Wang, Z., Lee, S. C., and Wang, T.: Revisiting nitrous acid (HONO) emission from on-road vehicles: A tunnel study with a mixed fleet, J. Air Waste Manage. Assoc., 67, 797-805, 10.1080/10962247.2017.1293573, 2017.

Lin, Y. L., Farley, R. D., and Orville, H. D.: BULK PARAMETERIZATION OF THE SNOW FIELD IN A CLOUD MODEL, Journal of Climate and Applied Meteorology, 22, 1065-1092, 10.1175/1520-0450(1983)022<1065:bpotsf>2.0.co;2, 1983.

Lu, K. D., Rohrer, F., Holland, F., Fuchs, H., Bohn, B., Brauers, T., Chang, C. C., Haeseler, R., Hu, M., Kita, K., Kondo, Y., Li, X., Lou, S. R., Nehr, S., Shao, M., Zeng, L. M., Wahner, A., Zhang, Y. H., and Hofzumahaus, A.: Observation and modelling of OH and HO2 concentrations in the Pearl River Delta 2006: a missing OH source in a VOC rich atmosphere, Atmospheric Chemistry and Physics, 12, 1541-1569, 10.5194/acp-12-1541-2012, 2012.

Ma, Q., Cai, S., Wang, S., Zhao, B., Martin, R. V., Brauer, M., Cohen, A., Jiang, J., Zhou, W., Hao, J., Frostad, J., Forouzanfar, M. H., and Burnett, R. T.: Impacts of coal burning on ambient PM2.5 pollution in China, Atmospheric Chemistry and Physics, 17, 4477-4491, 10.5194/acp-17-4477-2017, 2017.

Mao, J. Q., Ren, X. R., Chen, S. A., Brune, W. H., Chen, Z., Martinez, M., Harder, H., Lefer, B., Rappengluck, B., Flynn, J., and Leuchner, M.: Atmospheric oxidation capacity in the summer of Houston 2006: Comparison with summer measurements in other metropolitan studies, Atmospheric Environment, 44, 4107-4115, 10.1016/j.atmosenv.2009.01.013, 2010.

Meusel, H., Tamm, A., Kuhn, U., Wu, D., Leifke, A. L., Fiedler, S., Ruckteschler, N., Yordanova, P., Lang-Yona, N., Poehlker, M., Lelieveld, J., Hoffmann, T., Poeschl, U., Su, H., Weber, B., and Cheng, Y.: Emission of nitrous acid from soil and biological soil

crusts represents an important source of HONO in the remote atmosphere in Cyprus, Atmospheric Chemistry and Physics, 18, 799-813, 10.5194/acp-18-799-2018, 2018.

Mlawer, E. J., Taubman, S. J., Brown, P. D., Iacono, M. J., and Clough, S. A.: Radiative transfer for inhomogeneous atmospheres: RRTM, a validated correlated-k model for the longwave, Journal of Geophysical Research-Atmospheres, 102, 16663-16682, 10.1029/97jd00237, 1997.

Mlawer, E. J., and Clough, S. A.: Shortwave clear-sky model measurement intercomparison using RRTM, Proceedings of the 8 th Atmospheric Radiation Measurement (ARM) Science Team Meeting, Tucson, Arizona, USA, 1998.

Monge, M. E., D'Anna, B., Mazri, L., Giroir-Fendler, A., Ammann, M., Donaldson, D. J., and George, C.: Light changes the atmospheric reactivity of soot, Proceedings of the National Academy of Sciences of the United States of America, 107, 6605-6609, 10.1073/pnas.0908341107, 2010.

Ndour, M., D'Anna, B., George, C., Ka, O., Balkanski, Y., Kleffmann, J., Stemmler, K., and Ammann, M.: Photoenhanced uptake of NO2 on mineral dust: Laboratory experiments and model simulations, Geophysical Research Letters, 35, 10.1029/2007gl032006, 2008.

Oswald, R., Behrendt, T., Ermel, M., Wu, D., Su, H., Cheng, Y., Breuninger, C., Moravek, A., Mougin, E., Delon, C., Loubet, B., Pommerening-Roser, A., Sorgel, M., Poschl, U., Hoffmann, T., Andreae, M. O., Meixner, F. X., and Trebs, I.: HONO Emissions from Soil Bacteria as a Major Source of Atmospheric Reactive Nitrogen, Science, 341, 1233-1235, 10.1126/science.1242266, 2013.

Pan, Y. Y., Li, N., Zheng, J. Y., Yin, S. S., Li, C., Yang, J., Zhong, L. J., and Chen, D. H.: Emission inventory and characteristics of anthropogenic air pollutant sources in Guangdong Province Acta Scientiae Circumstantiae 35, 2655-2669, 2014.

Pathak, R. K., Wang, T., Ho, K. F., and Lee, S. C.: Characteristics of summertime PM2.5 organic and elemental carbon in four major Chinese cities: Implications of high acidity for water-soluble organic carbon (WSOC), Atmospheric Environment, 45, 318-325, 10.1016/j.atmosenv.2010.10.021, 2011.

Pathak, R. K., Wu, W. S., and Wang, T.: Summertime PM2.5 ionic species in four major cities of China: nitrate formation in an ammonia-deficient atmosphere, Atmospheric Chemistry and Physics, 9, 1711-1722, 10.5194/acp-9-1711-2009, 2009.

Qin, M., Xie, P. H., Su, H., Gu, J. W., Peng, F. M., Li, S. W., Zeng, L. M., Liu, J. G., Liu, W. Q., and Zhang, Y. H.: An observational study of the HONO-NO2 coupling at an urban site in Guangzhou City, South China, Atmospheric Environment, 43, 5731-5742, 10.1016/j.atmosenv.2009.08.017, 2009.

Ren, X. R., Harder, H., Martinez, M., Lesher, R. L., Oliger, A., Simpas, J. B., Brune, W. H., Schwab, J. J., Demerjian, K. L., He, Y., Zhou, X. L., and Gao, H. G.: OH and HO2 chemistry in the urban atmosphere of New York City, Atmospheric Environment, 37, 3639-3651, 10.1016/s1352-2310(03)00459-x, 2003.

Sarwar, G., Roselle, S. J., Mathur, R., Appel, W., Dennis, R. L., and Vogel, B.: A comparison of CMAQ HONO predictions with observations from the northeast oxidant and particle study, Atmospheric Environment, 42, 5760-5770, 10.1016/j.atmosenv.2007.12.065, 2008.

Stemmler, K., Ndour, M., Elshorbany, Y., Kleffmann, J., D'Anna, B., George, C., Bohn, B.,

and Ammann, M.: Light induced conversion of nitrogen dioxide into nitrous acid on submicron humic acid aerosol, Atmospheric Chemistry and Physics, 7, 4237-4248, 10.5194/acp-7-4237-2007, 2007.

Stutz, J., Alicke, B., Ackermann, R., Geyer, A., Wang, S. H., White, A. B., Williams, E. J., Spicer, C. W., and Fast, J. D.: Relative humidity dependence of HONO chemistry in urban areas, Journal of Geophysical Research-Atmospheres, 109, 10.1029/2003jd004135, 2004.

Su, H., Cheng, Y. F., Shao, M., Gao, D. F., Yu, Z. Y., Zeng, L. M., Slanina, J., Zhang, Y. H., and Wiedensohler, A.: Nitrous acid (HONO) and its daytime sources at a rural site during the 2004 PRIDE-PRD experiment in China, Journal of Geophysical Research-Atmospheres, 113, 10.1029/2007jd009060, 2008.

Su, H., Cheng, Y. F., Oswald, R., Behrendt, T., Trebs, I., Meixner, F. X., Andreae, M. O., Cheng, P., Zhang, Y., and Poschl, U.: Soil Nitrite as a Source of Atmospheric HONO and OH Radicals, Science, 333, 1616-1618, 10.1126/science.1207687, 2011.

Tan, J. H., Duan, J. C., He, K. B., Ma, Y. L., Duan, F. K., Chen, Y., and Fu, J. M.: Chemical characteristics of PM2.5 during a typical haze episode in Guangzhou, J. Environ. Sci., 21, 774-781, 10.1016/s1001-0742(08)62340-2, 2009.

Tham, Y. J., Wang, Z., Li, Q., Yun, H., Wang, W., Wang, X., Xue, L., Lu, K., Ma, N., Bohn, B., Li, X., Kecorius, S., Groess, J., Shao, M., Wiedensohler, A., Zhang, Y., and Wang, T.: Significant concentrations of nitryl chloride sustained in the morning: investigations of the causes and impacts on ozone production in a polluted region of northern China, Atmospheric Chemistry and Physics, 16, 14959-14977, 10.5194/acp-16-14959-2016, 2016.

VandenBoer, T. C.; Markovic, M. Z.; Sanders, J. E.; Ren, X.; Pusede, S. E.; Browne, E. C.; Cohen, R. C.; Zhang, L.; Thomas, J.; Brune, W. H.; Murphy, J. G.: Evidence for a nitrous acid (HONO) reservoir at the ground surface in Bakersfield, CA, during CalNex 2010, J. Geophys. Res. Atmos., 119, 9093–9106, doi:10.1002/2013JD020971, 2014

Wang, G., Zhang, R., Gomez, M. E., Yang, L., Zamora, M. L., Hu, M., Lin, Y., Peng, J., Guo, S., Meng, J., Li, J., Cheng, C., Hu, T., Ren, Y., Wang, Y., Gao, J., Cao, J., An, Z., Zhou, W., Li, G., Wang, J., Tian, P., Marrero-Ortiz, W., Secrest, J., Du, Z., Zheng, J., Shang, D., Zeng, L., Shao, M., Wang, W., Huang, Y., Wang, Y., Zhu, Y., Li, Y., Hu, J., Pan, B., Cai, L., Cheng, Y., Ji, Y., Zhang, F., Rosenfeld, D., Liss, P. S., Duce, R. A., Kolb, C. E., and Molina, M. J.: Persistent sulfate formation from London Fog to Chinese haze, Proceedings of the National Academy of Sciences of the United States of America, 113, 13630-13635, 10.1073/pnas.1616540113, 2016.

Wang, J., Zhang, X., Guo, J., Wang, Z., and Zhang, M.: Observation of nitrous acid (HONO) in Beijing, China: Seasonal variation, nocturnal formation and daytime budget, The Science of the total environment, 10.1016/j.scitotenv.2017.02.159, 2017a.

Wang, S. S., Zhou, R., Zhao, H., Wang, Z. R., Chen, L. M., and Zhou, B.: Long-term observation of atmospheric nitrous acid (HONO) and its implication to local NO2 levels in Shanghai, China, Atmospheric Environment, 77, 718-724, 10.1016/j.atmosenv.2013.05.071, 2013.

Wang, T., Lam, K. S., Lee, A. S. Y., Pang, S. W., and Tsui, W. S.: Meteorological and chemical characteristics of the photochemical ozone episodes observed at Cape

D'Aguilar in Hong Kong, Journal of Applied Meteorology, 37, 1167-1178, 10.1175/1520-0450(1998)037<1167:maccot>2.0.co;2, 1998.

Wang, T., and Kwok, J. Y. H.: Measurement and analysis of a multiday photochemical smog episode in the Pearl River delta of China, Journal of Applied Meteorology, 42, 404-416, 10.1175/1520-0450(2003)042<0404:maaoam>2.0.co;2, 2003.

Wang, T., Xue, L., Brimblecombe, P., Lam, Y. F., Li, L., and Zhang, L.: Ozone pollution in China: A review of concentrations, meteorological influences, chemical precursors, and effects, Science of the Total Environment, 575, 1582-1596, 10.1016/j.scitotenv.2016.10.081, 2017b.

Wang, X. M., Ding, X., Fu, X. X., He, Q. F., Wang, S. Y., Bernard, F., Zhao, X. Y., and Wu, D.: Aerosol scattering coefficients and major chemical compositions of fine particles observed at a rural site hit the central Pearl River Delta, South China, J. Environ. Sci., 24, 72-77, 10.1016/s1001-0742(11)60730-4, 2012.

Xu, J., Zhang, Y., and Wang, W.: Numerical study on the impacts of heterogeneous reactions on ozone formation in the Beijing urban area, Advances in Atmospheric Sciences, 23, 605-614, 10.1007/s00376-006-0605-1, 2006.

Xu, Z., Wang, T., Xue, L. K., Louie, P. K. K., Luk, C. W. Y., Gao, J., Wang, S. L., Chai, F. H., and Wang, W. X.: Evaluating the uncertainties of thermal catalytic conversion in measuring atmospheric nitrogen dioxide at four differently polluted sites in China, Atmospheric Environment, 76, 221-226, 10.1016/j.atmosenv.2012.09.043, 2013.

Xu, Z., Wang, T., Wu, J. Q., Xue, L. K., Chan, J., Zha, Q. Z., Zhou, S. Z., Louie, P. K. K., and Luk, C. W. Y.: Nitrous acid (HONO) in a polluted subtropical atmosphere: Seasonal variability, direct vehicle emissions and heterogeneous production at ground surface, Atmospheric Environment, 106, 100-109, 10.1016/j.atmosenv.2015.01.061, 2015.

Xue, L., Gu, R., Wang, T., Wang, X., Saunders, S., Blake, D., Louie, P. K. K., Luk, C. W. Y., Simpson, I., Xu, Z., Wang, Z., Gao, Y., Lee, S., Mellouki, A., and Wang, W.: Oxidative capacity and radical chemistry in the polluted atmosphere of Hong Kong and Pearl River Delta region: analysis of a severe photochemical smog episode, Atmospheric Chemistry and Physics, 16, 9891-9903, 10.5194/acp-16-9891-2016, 2016.

Xue, L. K., Wang, T., Gao, J., Ding, A. J., Zhou, X. H., Blake, D. R., Wang, X. F., Saunders, S. M., Fan, S. J., Zuo, H. C., Zhang, Q. Z., and Wang, W. X.: Ground-level ozone in four Chinese cities: precursors, regional transport and heterogeneous processes, Atmospheric Chemistry and Physics, 14, 13175-13188, 10.5194/acp-14-13175-2014, 2014.

Ye, C., Gao, H., Zhang, N., and Zhou, X.: Photolysis of Nitric Acid and Nitrate on Natural and Artificial Surfaces, Environmental Science & Technology, 50, 3530-3536, 10.1021/acs.est.5b05032, 2016a.

Ye, C., Zhang, N., Gao, H., and Zhou, X.: Photolysis of Particulate Nitrate as a Source of HONO and NOx, Environmental Science & Technology, 51, 6849-6856, 10.1021/acs.est.7b00387, 2017.

Ye, C. X., Zhou, X. L., Pu, D., Stutz, J., Festa, J., Spolaor, M., Tsai, C., Cantrell, C., Mauldin, R. L., Campos, T., Weinheimer, A., Hornbrook, R. S., Apel, E. C., Guenther, A., Kaser, L., Yuan, B., Karl, T., Haggerty, J., Hall, S., Ullmann, K., Smith, J. N., Ortega, J., and Knote, C.: Rapid cycling of reactive nitrogen in the marine boundary layer, Nature, 532, 489-491, 10.1038/nature17195, 2016b.

Yue, D. L., Zhong, L. J., Zhang, T., Shen, J., Zhou, Y., Zeng, L. M., Dong, H. B., and Ye, S. Q.: Pollution Properties of Water-Soluble Secondary Inorganic Ions in Atmospheric PM2.5 in the Pearl River Delta Region, Aerosol and Air Quality Research, 15, 1737-1747, 10.4209/aaqr.2014.12.0333, 2015.

Yun, H., Wang, Z., Zha, Q., Wang, W., Xue, L., Zhang, L., Li, Q., Cui, L., Lee, S., Poon, S. C. N., and Wang, T.: Nitrous acid in a street canyon environment: Sources and contributions to local oxidation capacity, Atmospheric Environment, 167, 223-234, 10.1016/j.atmosenv.2017.08.018, 2017.

Yun, H., Wang, W., Wang, T., Xia, M., Yu, C., Wang, Z., Poon, S. C. N., Yue, D., and Zhou, Y.: Nitrate formation from heterogeneous uptake of dinitrogen pentoxide during a severe winter haze in southern China, Atmos. Chem. Phys. Discuss., https://doi.org/10.5194/acp-2018-698, in review, 2018.

Zha, Q., Xue, L., Wang, T., Xu, Z., Yeung, C., Louie, P. K. K., and Luk, C. W. Y.: Large conversion rates of NO2 to HNO2 observed in air masses from the South China Sea: Evidence of strong production at sea surface?, Geophysical Research Letters, 41, 7710-7715, 10.1002/2014gl061429, 2014.

Zhang, L., Wang, T., Zhang, Q., Zheng, J., Xu, Z., and Lv, M.: Potential sources of nitrous acid (HONO) and their impacts on ozone: A WRF-Chem study in a polluted subtropical region, Journal of Geophysical Research-Atmospheres, 121, 3645-3662, 10.1002/2015jd024468, 2016.

Zhang, L., Li, Q. Y., Wang, T., Ahmadov, R., Zhang, Q., Li, M., and Lv, M. Y.: Combined impacts of nitrous acid and nitryl chloride on lower-tropospheric ozone: new module development in WRF-Chem and application to China, Atmospheric Chemistry and Physics, 17, 9733-9750, 10.5194/acp-17-9733-2017, 2017.

Zhang, Q., Streets, D. G., Carmichael, G. R., He, K. B., Huo, H., Kannari, A., Klimont, Z., Park, I. S., Reddy, S., Fu, J. S., Chen, D., Duan, L., Lei, Y., Wang, L. T., and Yao, Z. L.: Asian emissions in 2006 for the NASA INTEX-B mission, Atmospheric Chemistry and Physics, 9, 5131-5153, 10.5194/acp-9-5131-2009, 2009.

Zhang, Y. H., Su, H., Zhong, L. J., Cheng, Y. F., Zeng, L. M., Wang, X. S., Xiang, Y. R., Wang, J. L., Gao, D. F., Shao, M., Fan, S. J., and Liu, S. C.: Regional ozone pollution and observation-based approach for analyzing ozone-precursor relationship during the PRIDE-PRD2004 campaign, Atmospheric Environment, 42, 6203-6218, 10.1016/j.atmosenv.2008.05.002, 2008.

Zheng, B., Tong, D., Li, M., Liu, F., Hong, C., Geng, G., Li, H., Li, X., Peng, L., Qi, J., Yan, L., Zhang, Y., Zhao, H., Zheng, Y., He, K., and Zhang, Q.: Trends in China's anthropogenic emissions since 2010 as the consequence of clean air actions, Atmos. Chem. Phys., 18, 14095-14111, https://doi.org/10.5194/acp-18-14095-2018, 2018

Zheng, J., Zhong, L., Wang, T., Louie, P. K. K., and Li, Z.: Ground-level ozone in the Pearl River Delta region: Analysis of data from a recently established regional air quality monitoring network, Atmospheric Environment, 44, 814-823, 10.1016/j.atmosenv.2009.11.032, 2010.

Zhou, X. L., Gao, H. L., He, Y., Huang, G., Bertman, S. B., Civerolo, K., and Schwab, J.: Nitric acid photolysis on surfaces in low-NOx environments: Significant atmospheric implications, Geophysical Research Letters, 30, 10.1029/2003gl018620, 2003.

Zhou, X. L., Zhang, N., TerAvest, M., Tang, D., Hou, J., Bertman, S., Alaghmand, M., Shepson, P. B., Carroll, M. A., Griffith, S., Dusanter, S., and Stevens, P. S.: Nitric acid photolysis on forest canopy surface as a source for tropospheric nitrous acid, Nature Geoscience, 4, 440-443, 10.1038/ngeo1164, 2011.

Zou, Y., Deng, X. J., Zhu, D., Gong, D. C., Wang, H., Li, F., Tan, H. B., Deng, T., Mai, B. R., Liu, X. T., and Wang, B. G.: Characteristics of 1 year of observational data of VOCs, NOx and O-3 at a suburban site in Guangzhou, China, Atmospheric Chemistry and Physics, 15, 6625-6636, 10.5194/acp-15-6625-2015, 2015.

Tables

Table 1. Model performance of the default and revised CMAQ model for O_3, $PM_{2.5}$ and NO_2 at 56 monitoring sites in the PRD region

		OBS ($\mu g/m^3$)	SIM ($\mu g/m^3$)	Bias ($\mu g/m^3$)	NMB (%)	NME (%)	R
8h_max O_3	GEH (CMAQ-default)	84.79	56.55	-28.24	-33.3	42.69	0.29
	GEHRLPD (CMAQ-revised)		85.42	0.63	0.74	41.76	0.31
hourly $PM_{2.5}$	GEH (CMAQ-default)	78.75	72.34	-6.40	-8.13	46.6	0.60
	GEHRLPD (CMAQ-revised)		82.44	3.69	4.68	50.64	0.61
hourly NO_2*	GEH (CMAQ-default)	53.39	64.39	11.00	20.61	49.51	0.64
	GEHRLPD (CMAQ-revised)		58.42	5.03	9.42	43.75	0.67

*The NO_2 observation data were adjusted based on the method of Zhang et al. (2017): $NO_{2\,obs}=NO^{*}_{2\,obs}\times\frac{NO_{2\,sim}}{NO_{2\,sim}+NO_{z\,sim}-Nitrate_{sim}}$, where $NO^{*}_{2\,obs}$ is the measured concentration of NO_2 by the catalytic conversion technique; $NO_{2\,sim}$, $NO_{z\,sim}$ and $Nitrate_{sim}$ are the simulated concentrations of NO_2, NO_Z and nitrate.

Figure Captions

Fig.1. Model domains and locations of the monitoring sites. Green star represents Heshan site and red dots represent official monitoring sites in the PRD region from the Ministry Environmental Protection of China

Fig.2. Observed and simulated HONO mixing ratios by the default and revised CMAQ model at Heshan site during 4-8 January 2017.

Fig.3. Average diurnal variations of contributions of different HONO sources to the simulated HONO mixing ratios at Heshan site for 4-8 January 2017. The HONO sources include gas-phase homogeneous reaction of NO and OH (G), vehicle emissions (E), heterogeneous reactions under dark condition with the RH of 50% (H), RH-enhancing effects on heterogeneous reactions (R), light-enhancing effects on heterogeneous reactions (L), photolysis of particulate nitrate in the atmosphere (P) and photolysis of HNO_3/nitrate deposited on the surface (D)

Fig.4. Average diurnal variations of OH and HO_2 mixing ratios simulated in the NO_HONO and GEHRLPD case at Heshan site during 4-8 January 2017.

Fig.5. Average diurnal variations of contributions of different reactions to HO_X generation at Heshan site.

Fig.6. Temporal variation of observed and simulated O_3 mixing ratios in the NO_HONO and GEHRLPD case at Heshan site during 4-8 January 2017.

Fig.7. Spatial distributions of O_3 mixing ratios at 15:00 LTC simulated in the NO_HONO and GEHRLPD case, and their difference for domain 3.

Fig.8. Temporal variation of observed and simulated total nitrate, sulfate, and ammonium concentrations in the NO_HONO and GEHRLPD case at Heshan site during 4-8 January 2017.

Fig.9 Spatial distributions of average TNO_3 concentrations simulated in the NO_HONO and GEHRLPD case, and their difference for domain 3 during 4-8 January 2017.

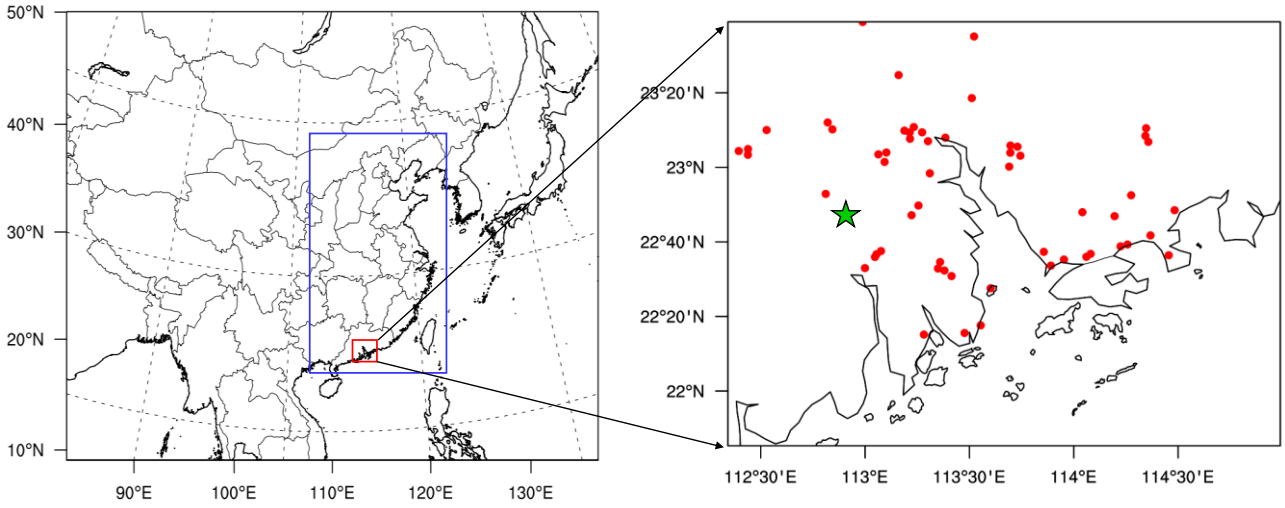

Fig.1. Model domains and locations of the monitoring sites. Green star represents Heshan site and red dots represent official monitoring sites in the PRD region from the Ministry Environmental Protection of China

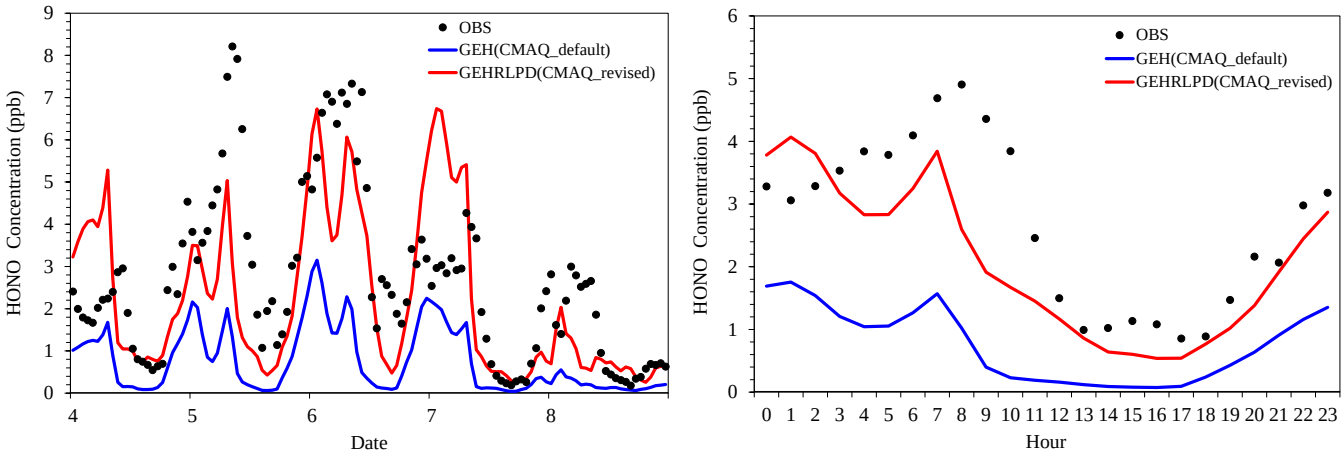

Fig.2. Observed and simulated HONO mixing ratios by the default and revised CMAQ model at Heshan site during 4-8 January 2017.

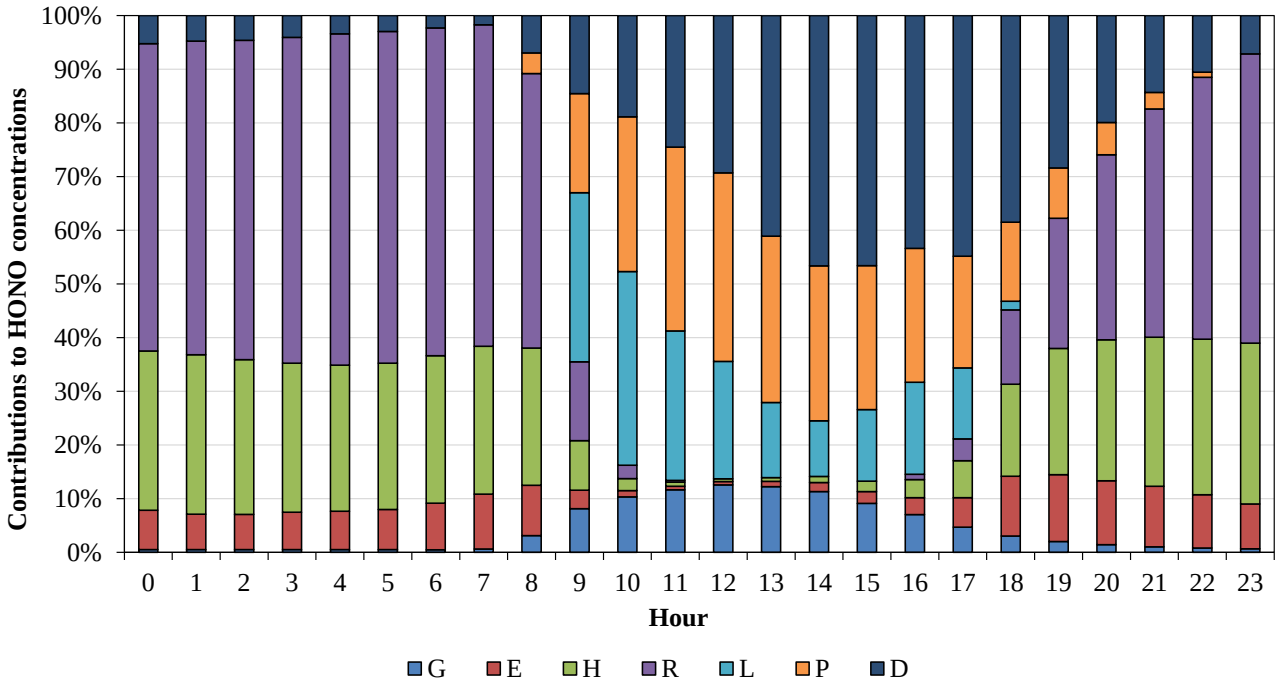

Fig.3. Average diurnal variations of contributions of different HONO sources to the simulated HONO mixing ratios at Heshan site for 4-8 January 2017. The HONO sources include gas-phase homogeneous reaction of NO and OH (G), vehicle emissions (E), heterogeneous reactions under dark condition with the RH of 50% (H), RH-enhancing effects on heterogeneous reactions (R), light-enhancing effects on heterogeneous reactions (L), photolysis of particulate nitrate in the atmosphere (P) and photolysis of HNO_3/nitrate deposited on the surface (D)

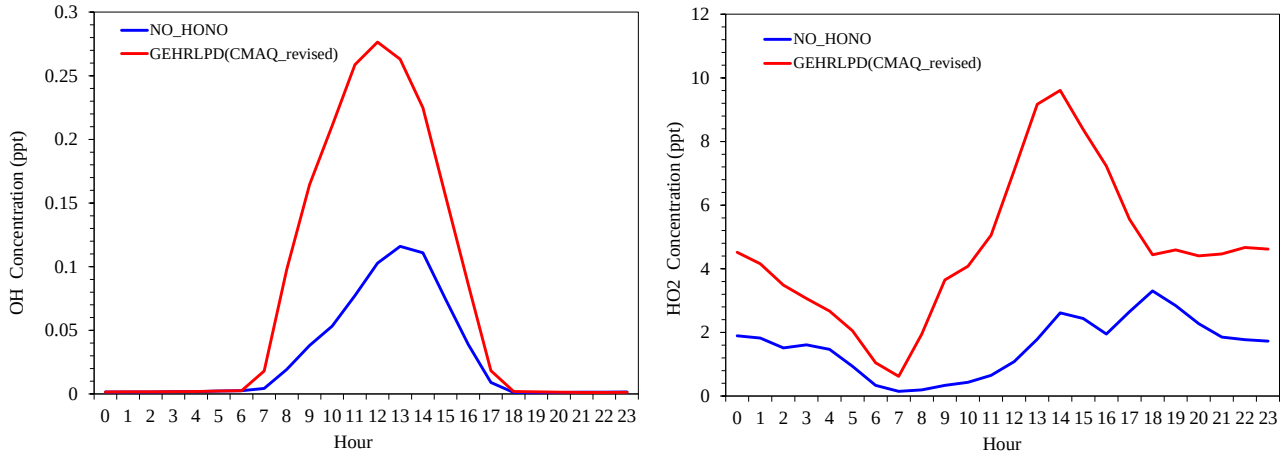

Fig.4. Average diurnal variations of OH and HO_2 mixing ratios simulated in the NO_HONO and GEHRLPD case at Heshan site during 4-8 January 2017.

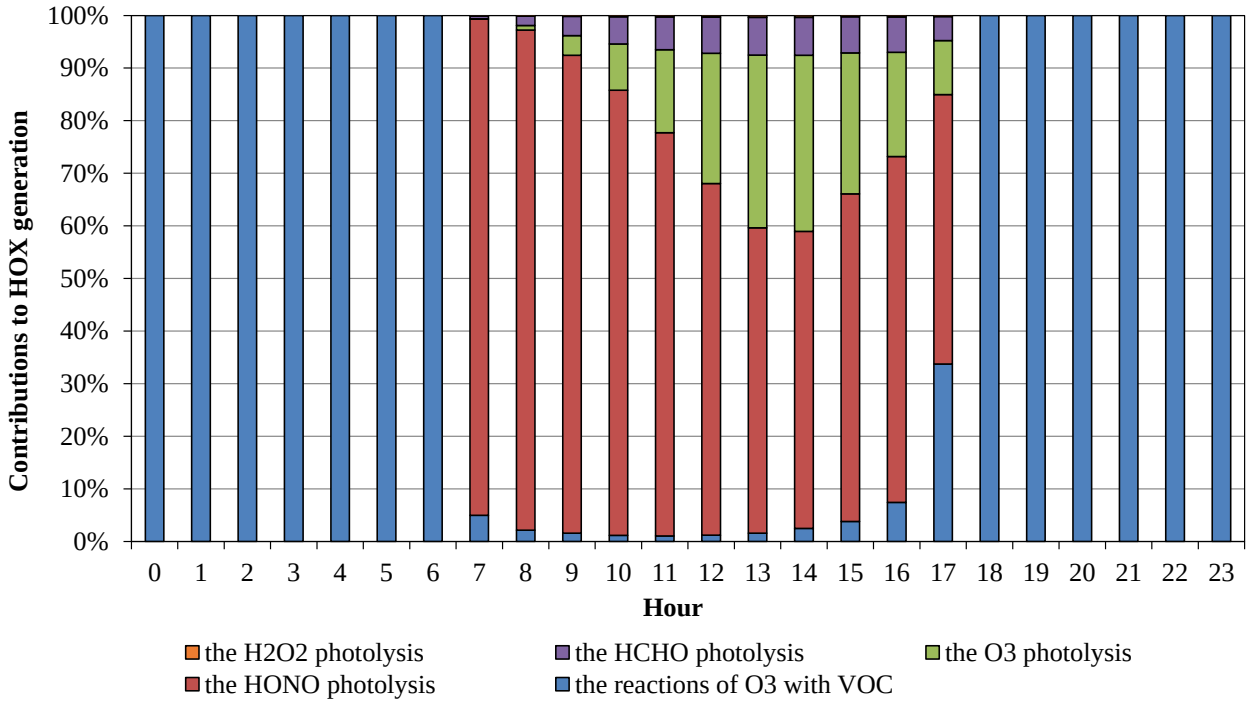

Fig.5. Average diurnal variations of contributions of different reactions to HO_X generation at Heshan site.

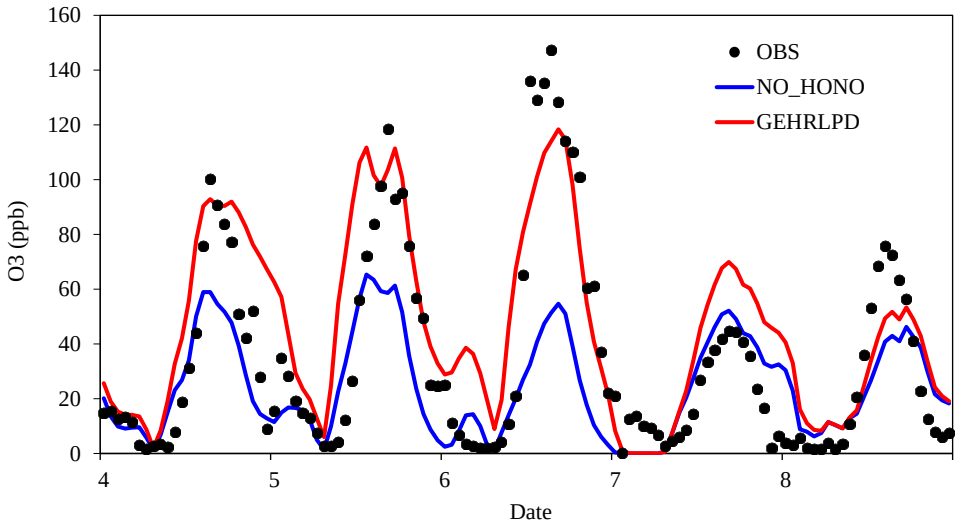

Fig.6. Temporal variation of observed and simulated O_3 mixing ratios in the NO_HONO and GEHRLPD case at Heshan site during 4-8 January 2017.

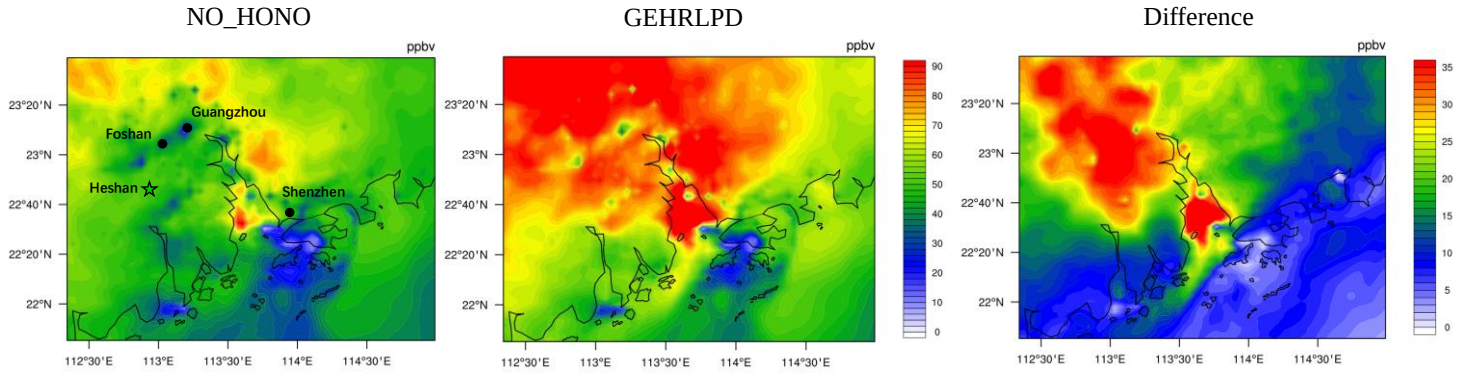

Fig.7. Spatial distributions of O_3 mixing ratios at 15:00 LTC simulated in the NO_HONO and GEHRLPD case, and their difference for domain 3.

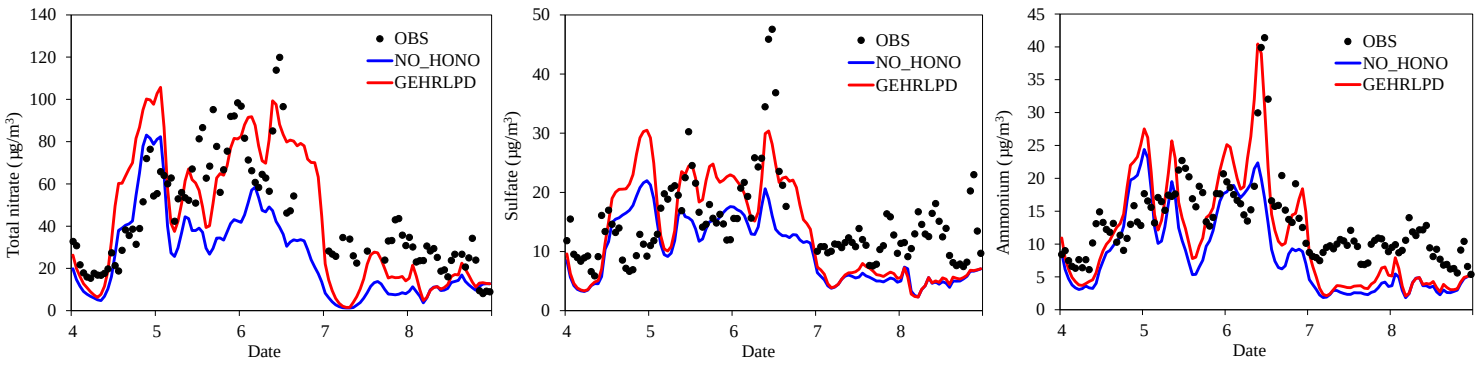

Fig.8. Temporal variation of observed and simulated total nitrate, sulfate, and ammonium concentrations in the NO_HONO and GEHRLPD case at Heshan site during 4-8 January 2017.

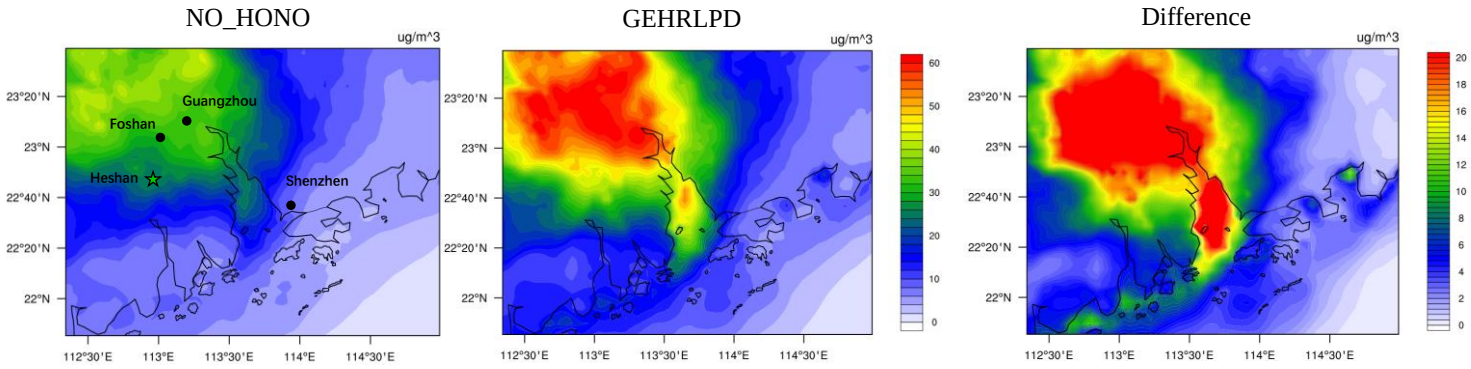

Fig.9 Spatial distributions of average TNO_3 concentrations simulated in the NO_HONO and GEHRLPD case, and their difference for domain 3 during 4-8 January 2017.